Vol. 80 (1991) *ACTA PHYSICA POLONICA A* No 2

Proceedings of the XX International School of Semiconducting Compounds, Jaszowiec 1991

FOUR- AND TWO-WAVE MIXING IN SOLIDS

A. SUCHOCKI

Center for Laser Research, Oklahoma State University
Stillwater, Oklahoma 74078, USA
and
Insitute of Physics, Polish Academy of Sciences
Al. Lotników 32/46, 02–668 Warszawa, Poland

G.D. GILLILAND*, G.J. QUARLES†, M.S. PETROVIC* AND R.C. POWELL

Center for Laser Research, Oklahoma State University
Stillwater, Oklahoma 74078, USA

The paper gives an overview of theory and presents several examples of application of some holographic techniques: four-wave mixing, self-scattering and beam coupling to study nonlinear optical properties of solids. Among them excitation energy transfer in chromium-doped vibronic laser materials and picosecond study of undoped CdTe are reported.

PACS numbers: 42.65.Ma, 71.35.+z

1. Introduction

Nonlinear optics is one of the fastest-developing part of physics, very closely related to applications. The most often used experimental methods of nonlinear optics involve crossing of various laser beams in examined materials. The crossing of two and more laser beams in suitable materials can lead to a number of phenomena, which can be treated theoretically as third order nonlinear processes [1–3]. As a result of such interaction new laser beams can be produced, travelling in different directions than the original beams and having different frequencies. The possible range of application of these phenomena is very broad. They can be

*Present address: IBM Thomas J. Watson Research Center, P.O. Box 218, Yorktown Heights, N.J. 10598, USA

†Present address: Naval Research Laboratories, Code 6551, Washington, D.C., 20375–5000, USA

used to produce optical switches, to make new optical resonators and other optical devices, in real-time holography, image processing, object tracing, nuclear fusion, etc. They are also used to study the interactions of light with matter and as a spectroscopic tool to examine some properties of solids, hardly accessible by other spectroscopic techniques.

The goal of this paper is to give an overview of the theory and experimental techniques, such as four wave-mixing (FWM), self-scattering and two-beam coupling, and to present examples of application of these techniques to study the excitation energy transfer phenomena in vibronic laser materials and nonlinear properties of semiconductors, especially CdTe.

Several physical processes can lead to the obtaining of FWM phenomena through laser-induced spatial modulation of the materials complex refractive index. Among the most commonly observed are thermal, electro-optical, structural, concentration and population effects. Each of these have different characteristic in terms of response times and sensitivities, which allows to distinguish clearly the type of effect responsible for the spatial modulation of the refractive index of the examined material. Population effects, including population of excited ions, free carriers, trapped carriers, etc. are very often a source of light-induced gratings in solids.

2. Population gratings of excited states of ions

Measurements of light-induced gratings of excited states of dopant ions in solids are a very convenient way of examining the excitation energy migration among the dopant ions. Therefore, this method has been applied in many works. It has been used to verify the occurrence of excitation energy migration among Cr^{3+} ions in ruby [4–6]. The results of FWM studies definitely confirmed the lack of long-range energy migration in this material. These findings have been followed by theoretical studies which explained the observed results [7–9]. It was, therefore, important to check if the excitation energy migration occurs in other systems with chromium.

Various types of experimental setups have been used to study this phenomenon. They always involve crossing of two coherent laser beams (so-called write beams), which are in resonance with internal optical transitions of dopant ions to create an interference pattern in the sample. In this case a sinusoidal pattern of excited states of dopant ions arises in the same place as the original interference pattern of the interfering beams. This forms the light-induced holographic gratings due to differences in the polarizability of ions in ground and excited states. The grating fringe separation Λ can be easily controlled by changing the crossing angle between the two write beams Θ and can be expressed by the formula:

$$\Lambda = \frac{\lambda_p}{2\sin(\Theta/2)}, \tag{1}$$

where λ_p is the wavelength of the write beams. Both λ_p and Θ are measured in the air. The created gratings are probed by the third beam, either of the same or

different wavelength as the write beams. In the former case the experiment is called degenerate FWM (DFWM), in the latter non-degenerate FWM (NDFWM). The third beam is directed at the Bragg angle to the grating (counter-propagating or almost counter-propagating to one of the write beams, in the case of DFWM and NDFWM, respectively). Due to scattering of the probe beam the fourth, signal beam arises, which travels counter-propagating (almost counter-propagating) to the other write beam.

The scattering efficiency η of the thick hologram formed in this way depends on the differences of the light-induced changes in the absorption coefficient $\Delta\alpha$ or differences in the refractive index Δn between the peaks and the valleys of the grating and is given in the first approximation by Kogelnik's formula [10]:

$$\eta = \mathrm{e}^{-2\alpha\Gamma}\left[\sinh^2(\Delta\alpha\Gamma/2) + \sin^2(\pi\Delta n\Gamma/\lambda)\right], \tag{2}$$

where $\Gamma = d/\cos\Theta$ with d being the hologram thickness and α is the average absorption coefficient at the laser wavelength λ. The peak-to-valley difference in the absorption coefficient, in the simplest approximation which involves only two levels, is equal to [11]:

$$\Delta\alpha = [N_0 I_0 \sigma_1(\sigma_2 - \sigma_1)] / (2I_0\sigma_1 + h\nu/\tau), \tag{3}$$

where N_0 is the total concentration of the dopant, I_0 is the energy density of the laser pump beams of photon energy $h\nu$, τ is the luminescence decay time of the excited state, and σ_1 and σ_2 are the absorption cross sections of the ground and excited states at wavelength λ. Much more difficult to calculate are the peak-to-valley changes in the refractive index since the contribution from all possible transitions of the dopant ions in the ground and metastable states should be taken into account. In the two-level approximation they should be also proportional to the population of the excited state $N_{2\mathrm{p}}$ expressed by:

$$N_{2\mathrm{p}} = 2I_0 N_0 \sigma_1 / (2I_0\sigma_1 + h\nu/\tau). \tag{4}$$

The information on excitation energy migration can be obtained by monitoring the decay kinetics of laser-induced population gratings. In the simple case of diffusive energy migration among one type of ions, the decay kinetics should be single exponential with a decay rate K given by [12]:

$$K = 2\tau^{-1} + [32(\pi/\lambda)^2 \sin^2(\Theta/2)]\, D. \tag{5}$$

The first term describes the destruction of the grating due to the fluorescence decay of the ions in the excited state (see Fig. 1). The second term describes the destruction of the grating due to migration of the excitation energy from ions in the peak to ions in the valley region of the grating. The last term depends on the diffusion coefficient of the energy migration D and on the grating spacing Λ. Thus, by measuring the FWM signal decay rate as a function of the write-beam crossing angle, it is possible to determine the energy diffusion coefficient. In case of several non-interacting types of ions or different sites the decay kinetics should be a sum of individual exponential components.

In the case of very long mean-free-path energy migration (partially coherent or coherent energy migration), the FWM signal is no longer exponential. In such a

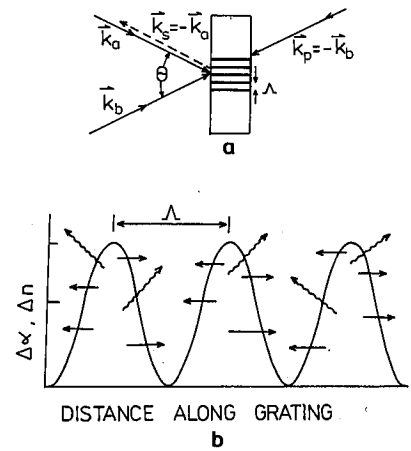

Fig. 1. (a) Laser beam alignment for degenerate four-wave mixing. (b) Laser-induced grating pattern and mechanisms of decay: (∿∿∿→) — radiative decay of excited ions, (→) — energy migration from peak to valley region of grating.

case the FWM signal kinetics are described by the theory of Kenkre. In this model the time dependence of the normalized FWM signal is given by [13, 14]:

$$I_s(t) = e^{-2t/\tau}\left\{J_0(bt)e^{-\beta t} + \beta\int_0^\infty du\, e^{-\beta(t-u)}J_0(b(t^2-u^2)^{1/2})\right\}^2, \qquad (6)$$

where β is the exciton (in Frenkel's sense) scattering rate, J_0 is the Bessel function of order zero and b is equal to [13]:

$$b = 4V\sin[(2\pi a/\lambda)\sin(\Theta/2)], \qquad (7)$$

where V is the nearest-neighbor ion–ion interaction rate, and a is average distance between active ions. The exciton dynamics (i.e. the diffusion coefficient D, the mean free path L_m, the diffusion length L_D, the coherence parameter ζ and the number of sites visited between scattering events N_s) are expressed via the above given parameters in the following way [13]:

$$D = 2V^2a^2/\beta, \qquad (8)$$

$$L_m = \sqrt{2Va/\beta}, \qquad (9)$$

$$L_D = \sqrt{2D\tau}, \qquad (10)$$

$$\zeta = b/\beta, \qquad (11)$$

$$N_s = L_m/a. \qquad (12)$$

The transport properties of excitons are discernible with use of the FWM technique if the diffusion length and grating spacing are on the same length scale.

It should be pointed out that in the case of partially coherent or coherent energy migration a better insight into the microscopic parameters of energy migration, L_m, L_D, D and N_s, could be obtained than in the case of diffusive, incoherent exciton motion, which yields only the value of D. The term "coherence" in this case describes the situation in which the exciton behaves like a quasiparticle with a certain momentum. This quasiparticle will move over several lattice spacings, maintaining phase memory, before a scattering event occurs. The type of exciton motion could be classified by comparison of the mean free path L_m, ion–ion distance a, and the grating spacing Λ [15]. Table shows this classification.

TABLE

Classification of transport properties of excitons, measured in the FWM experiments.

a, L_m and Λ comparison	Type of exciton motion
$L_m \leq a$	completely incoherent
$a < L_m \ll \Lambda/2$	coherent over a few lattice spacing, incoherent on the scale of experiment
$L_m \approx \Lambda/2$	partially coherent
$L_m \geq \Lambda/2$	coherent

Information on the interaction mechanisms responsible for the energy transfer and exciton scattering could be obtained by measuring the temperature dependencies of the microscopic parameters of exciton migration. The results of the FWM energy transfer study in emerald will serve as an example of such measurements.

3. FWM measurements of excitation energy migration in emerald

The experimental setup in the NDFWM measurements of emerald with chromium concentration about 3 at. % is shown in Fig. 2 [16]. Crossed laser beams from a ring dye laser were tuned to 588 nm, in order to pump resonantly the $^4T_2$ band. This established a population grating of excited Cr^{3+} ions in the sample. A He–Ne laser was used as the probe beam and the signal beam was processed by a signal averager. The FWM decay kinetics were found to be non-exponential and dependent on the crossing angle of the write beams at all temperatures for which a signal was visible [17]. The signal kinetics are consistent with the predictions of the theory of Kenkre, indicating the presence of long mean-free-path exciton migration. The kinetics were fitted using Eq. (6), treating b and β as adjustable parameters. Figure 3 shows the temperature dependencies of the ion–ion interaction rate and the scattering rate [17]. Both β and V increase with temperature in the measured range. The increase in the former of β can be attributed to enhanced scattering by acoustic phonons, which increases as $T^{3/2}$ [18] and is shown by the dashed line in Fig. 3(a). The temperature dependence of V can be attributed to the relative increase in the vibronic sideband emission compared to the R-line

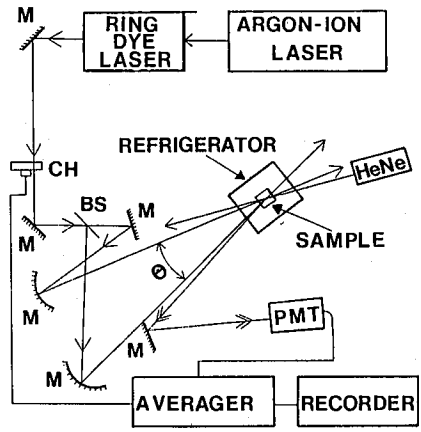

Fig. 2. Schematic representation of the NFWM setup: PMT — photomultiplier, CH — chopper, M — mirror, BS — beam splitter.

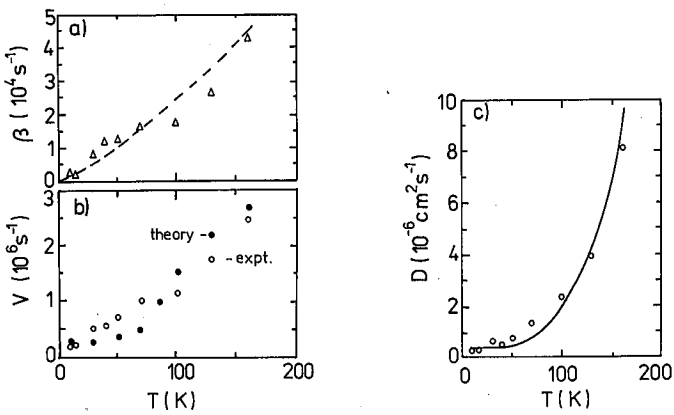

Fig. 3. The temperature dependence of (a) the exciton scattering rate β, (b) the ion–ion interaction rate V and (c) the exciton diffusion coefficient D obtained from the FWM measurements of emerald. The lines in (a) and (c) represent the theoretical predictions.

emission. This causes an increase in the overlap between the emission and absorption spectra and an increase of the total emission rate. Both these factors cause the ion–ion interaction rate to increase. This can be approximated by

$$V(T) = C\tau^{-1}(I_{\mathrm{vib}}/I_{\mathrm{R}}), \tag{13}$$

where I_{vib} and I_{R} represent the intensities of the two components of the fluorescence spectrum and C is a proportionality constant. Using the values of the relative intensities and the fluorescence lifetimes measured experimentally in Eq. (13) gives the theoretical points shown in Fig. 3(b), which are in good agreement

with the experimentally determined temperature dependence for V. Applying Eq. (8), the diffusion coefficient for long-range resonant exciton migration can be determined. Fig. 3(c) shows the results obtained using the experimental points for V and β. The solid line in the figure is obtained using the theoretical curves given in Figs. 3(a) and 3(b). There is a good agreement between the two results.

The long-range excitation energy migration has also been found for chromium ions in mirror sites of alexandrite crystals with use of the same technique. These results have been independently confirmed by the group of Kaplyanskii [19]. They used pseudo-Stark effect to examine the energy transfer properties of chromium ions in alexandrite crystals. However, the temperature dependence of D is quite different in alexandrite and emerald. Though in both materials the scattering rate limiting the mean-free-path of the excitons was found to increase with temperature, at low temperatures the ion–ion interaction rate in alexandrite is independent of temperature [15], whereas in emerald it increases with temperature [17]. This is because the vibronic emission transitions become important at much lower temperatures in emerald than in alexandrite, as can be seen from their fluorescence spectra. This is associated with the weaker crystal field at the site of the Cr^{3+} ion in the emerald host compared to alexandrite.

It is impossible to explain the observed ion–ion interaction rates between chromium ions assuming the dipole–dipole mechanism of interaction in materials studied. Most probably the exchange or superexchange interaction mechanism dominates the interaction between Cr^{3+} ions in the emerald and alexandrite crystals [15–17].

4. DFWM measurements of undoped cadmium telluride

The determination of the diffusion coefficient of an excited state is very important to clarify the scattering and energy transfer mechanism of an excited state in semiconductors. In the case of the excited state of a charged particle like an electron and a hole, the scattering mechanism is easily studied by measuring the Hall effect or the drift mobility. However, for an electrically neutral excited state like an exciton or an excitonic molecule, it is very often impossible to study the scattering mechanism by conventional electrical methods. The transient grating method has following advantages [20]:

— the determination simultaneously the diffusion coefficient and the lifetime of the excited state without any electrodes;

— the determination the diffusion coefficient and the lifetime in a small area and to get topographical information on the diffusion coefficient and the lifetime;

— the determination the surface recombination rates.

Dynamics holographic gratings were first observed in semiconductors by Woerdman and Bolger [21] in Si and first studied in CdTe by Kremenitskij, Odulov and Soskin [22]. The DFWM picosecond pulse-probe technique was used to determine the nonlinear optical responses due to free carriers. The ambipolar diffusion coefficient D_a, free-carrier lifetime τ_{FC}, and laser-induced changes in the refractive index Δn were found for various undoped samples of CdTe. The gratings were

produced by two-phonon absorption of 30 ps (full width at half maximum) pulses of Nd:YAG laser at 1.064 μm. The grating has been probed by the split-off weak pulse of the same laser, delayed with respect to the two write pulses by an optical delay line. Such a procedure allowed to probe the light-induced grating up to a few nanoseconds. The decay rates of the DFWM signal are described by Eq. (5) with the free-carrier lifetime τ_{FC} in place of the decay time. Figure 4 shows the observed decay rates of the DFWM signal of the p-type CdTe sample [23]. The

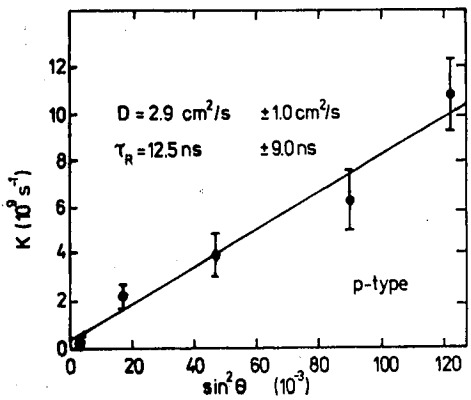

Fig. 4. Laser-induced grating decay rate K in p-type sample of CdTe as a function of write beam crossing angle.

straight line shows the best fit to the data. The intercept of this line with the decay rate axis gives the value of $2/\tau_{FC}$ and the slope is equal to $32\pi^2 D_a/\lambda^2$. The ambipolar diffusion coefficient is defined as [24]:

$$D_a = 2[(D_e D_h)/(D_e + D_h)], \tag{14}$$

where

$$D_{e,h} = \mu_{e,h}(k_B T/e). \tag{15}$$

The last equation is the Einstein relationship between the electron–hole diffusion coefficient and mobilities $\mu_{e,h}$ at temperature T, e is the modulus of the electronic charge and k_B is the Boltzmann's constant. The measured value of D_a being equal to 2.9 ± 1 cm^2/s is in good agreement with that calculated from the Einstein formula, $D_a^{th} = 4.3$ cm^2/s [23].

5. Self-scattering in CdTe

At sufficiently small write angles, multiple diffracted orders are observed on the side of the sample opposite to that of the two incident write beams, as schematically depicted in Fig. 5. This effect, first observed in semiconductors by

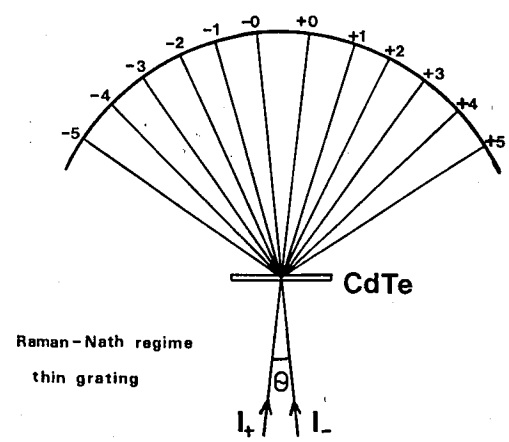

Fig. 5. The schematic representation of Raman–Nath diffraction, or self-scattering.

Woerdman and Bolger [21], is known as self-scattering, or Raman–Nath scattering [25], and defines the "thin grating" regime [26]. The scattering efficiency of the i-th order in the case of equal write beam intensities is given by [25]:

$$\eta_i = A[J_i^2(\gamma\Delta n) + J_{i+1}(\gamma\Delta n)], \tag{16}$$

where

$$\gamma = 2\pi d/\lambda \cos\Theta_{\text{xtal}}. \tag{17}$$

Here A is a constant of proportionality, d is the grating thickness, Δn are the induced changes in the refractive index, Θ is the crossing angle inside the material and J_i is the Bessel function of integer order i. Figure 6 [23] shows an example of the relative intensities of the diffracted orders versus order. A computer fit of Eq. (16) to the data, treating A and Δn as adjustable parameters, gives the free-carrier induced change in the refractive index. In the p-type sample it was found that $\Delta n = 4.6 \times 10^{-4}$. This value can be also estimated from the Drude model. This estimation gives the value of Δn being equal to 0.7×10^{-4}, which is less than the value obtained from the self-scattering experiment. This may be related to the fact, that the total free-carrier distribution in the sample is greater than the Drude model estimate due to additional effects associated with the detailed band structure of the material. Thus, this corroborates the assumption that the signal observed is caused a distribution of free carriers [23].

6. Beam coupling (two-wave mixing)

In one of the most commonly used method to probe nonlinear optical properties of a material, induced by charge redistribution in the material, two write beams of unequal intensity intersect inside the sample to form a spatially sinusoidal

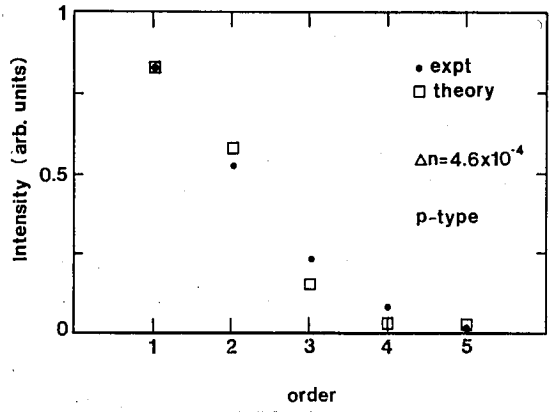

Fig. 6. The self-scattering signal intensity of the first five diffracted orders for p-type sample of undoped CdTe. (• — experimental points, [] — the fit of the Raman–Nath theory to the data).

interference pattern. In the region of constructive interference the charge carriers are excited to the band states, undergo diffusion, electric field-induced drift and the so-called photovoltaic effect (i.e. directionally preferential drift along the direction of polar axis), and finally may be recaptured by traps. Anisotropic electron trapping and ion displacement may also contribute to the photocurrent [27]. The above effects result in charge redistribution and give rise to the space-charge field. This field, acting through the linear electrooptic effect, modulates the refractive index of the material. If the grating is displaced with respect to the incident optical interference pattern the beam coupling gives rise to energy transfer from one beam to the other. This effect has been first observed in semiconductors by Klein (in undoped semi-insulating GaAs) [28]. The direction of such energy transfer is dependent on the crystal orientation and the sign of the photo-carrier charge but not on the relative write beam intensity.

The picosecond beam coupling was observed in undoped CdTe crystals with practically no midgap linear absorption under Nd:YAG 1.064 μm laser excitation [29]. The two-photon absorption produced electron–hole plasma. The coupling proceeds through the so-called Dember effect [30] (excited carriers separation due to large differences in electron and hole mobilities), which induced the phase-shifted holographic grating in the crystal. The experimental geometry used in the experiment is shown in Fig. 7 [29].

The quantity measured here is $\Delta T/T_0 = (T - T_0)/T_0$, where T and T_0 are the probe beam transmissions in the presence and absence of the pump beam, respectively. The theoretical values of the transmission in either case is obtained by solving numerically the coupled rate and optical field equations. $\Delta T/T_0$ can be expressed as [27]:

$$\Delta T/T_0 = [\exp(-\alpha l \pm \Delta\alpha l + \Gamma l) - \exp(-\alpha l)]/\exp(-\alpha l), \tag{18}$$

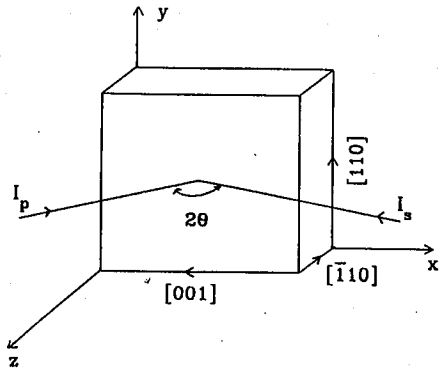

Fig. 7. The experimental geometry used in the beam-coupling experiment in CdTe (I_p — the pump beam, I_s — the probe beam).

where the αl term represents the probe absorption independent of the pump, $\Delta\alpha l$ represents the probe absorption that depends on the pump (which may be due to processes such as saturable absorption, two-photon absorption, transient energy transfer or absorption gratings) and Γl represents the probe photorefractive gain that depends on the pump. Since the photorefractive gain is dependent on crystal orientation, it can be separated from the isotropic contributions of probe gain or loss by measuring $\Delta T/T_0$ in two orientations — one differing from the other by a 180° rotation about the write beam angle bisector. Figure 8 [29] shows the results of picosecond beam coupling in a high-resistivity p-type sample of CdTe. The open circles denote the measured values of $\Delta T/T_0$ for the orientation where

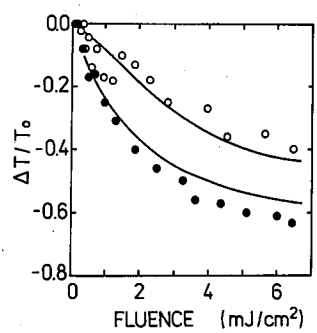

Fig. 8. Results of picosecond beam coupling as a function of total fluence for copolarized write beams. The solid lines represent the theoretical fits.

energy transfer is from pump to probe, while the solid circles denote $\Delta T/T_0$ for the orientation where the transfer is from probe to pump. The solid lines indicate the fits of solutions of the rate and optical field equations to the data, with the values of electro-optic coefficient being equal to $r_{41} = 10$ pm/V and two-photon

absorption coefficient $\beta_{TPA} = 50$ cm/GW. The obtained theoretical curves fit the experimental data very well. No cw beam-coupling has been observed in the sample for irradiances in the 10 W/cm^2 range [29].

7. Other holographic experiments in semiconductors

Several other experiments involving holographic gratings have been performed in semiconductor materials. Among them the polarization rotation of the probe beam in CdTe was studied [29]. Recently, the holographic gratings have been also applied to study magnetoresistance and magnetocapacitance oscillations in AlGaAs/GaAs heterojunctions [31–33]. It should be also mentioned that this method is most commonly used to study the whole class of photorefractive materials [27]. The number of possible applications of such techniques, both as a tool to study the basic properties of materials and in practical applications, seems to be very large.

References

[1] R.A. Fisher (Ed.), *Optical Phase Conjugation*, Academic Press, New York 1983.

[2] H.J. Eichler, P. Gunter, D.W. Pohl, *Laser-Induced Dynamic Gratings*, Springer-Verlag, Berlin 1986.

[3] B.Yu. Zeldowich, N.F. Filipetskii, V.V. Shkunov, *Obrashchenie volnovogo fronta*, Nauka, Moskwa 1985.

[4] H.J. Eichler, J. Eichler, J. Knof, Ch. Noack, *Phys. Status Solidi A* **52**, 481 (1979).

[5] D.S. Hamilton, D. Heiman, J. Feinberg, R.W. Hellwarth, *Opt. Lett.* **4**, 124 (1979).

[6] P.F. Liao, L.M. Humphrey, D.M. Bloom, S. Geschwind, *Phys. Rev. B* **20**, 4145 (1979); P.F. Liao, D. Bloom, *Opt. Lett.* **3**, 4 (1978).

[7] S. Chu, H.M. Gibbs, A. Passner, *Phys. Rev. B* **24**, 7162 (1981).

[8] W.Y. Ching, D.L. Huber, *Phys. Rev. B* **25**, 1096 (1982).

[9] D.L. Huber, W.Y. Ching, *Phys. Rev. B* **25**, 6472 (1982).

[10] H. Kogelnik, *Bell Syst. Tech. J.* **48**, 2909 (1969).

[11] K.O. Hill, *Appl. Opt.* **10**, 1695 (1971).

[12] J.R. Salcedo, A.E. Siegman, D.D. Dlott, M.D. Fayer, *Phys. Rev. Lett.* **41**, 131 (1978).

[13] V.M. Kenkre, D. Schmid, *Phys. Rev. B* **31**, 2430 (1985).

[14] Y.M. Wong, V.M. Kenkre, *Phys. Rev. A* **22**, 3072 (1980).

[15] G.D. Gilliland, A. Suchocki, K.W. Ver Steeg, R.C. Powell, *Phys. Rev. B* **38**, 6227 (1988).

[16] A. Suchocki, G.D. Gilliland, R.C. Powell, *Phys. Rev. B* **35**, 5830 (1987).

[17] G.J. Quarles, A. Suchocki, R.C. Powell, *Phys. Rev. B* **38**, 9996 (1988).

[18] V.M. Agranovich, M.D. Galanin, *Electronic Excitation Energy Transfer in Condensed Matter,* North-Holland, Amsterdam 1982; V.M. Agranovich, Yu. V. Konobeev, *Opt. Spektrosk.* **6**, 642 (1959); **6**, 648 (1959) [*Opt. Spectrosc.* (USSR) **6**, 155 (1959); **6**, 421 (1959)]; *Phys. Status Solidi* **27**, 435 (1968).

[19] S.A. Basun, S.P. Feofilov, A.A Kaplyanskii, *J. Lumin.* **48&49**, 166 (1991).

[20] Y. Aoyagi, Y. Segawa, S. Namba, *IEEE J. Quantum Electron.* **QE-22**, 1320 (1986).

[21] J. Woerdman, B. Bolger, *Phys. Lett A* **30**, 164 (1969).

[22] V. Kremenitskii, S. Odulov, M. Soskin, *Phys. Status Solidi A* **51**, K63 (1979).

[23] M.S. Petrovic, A. Suchocki, R.C. Powell, G. Cantwell, J. Aldridge, *J. Appl. Phys.* **66**, 1359 (1989).

[24] C. Kittel, *Introduction to Solid State Physics,* Wiley, New York 1966.

[25] C. Raman, N. Nath, *Proc. Indian Acad. Sci.* **2**, 413 (1935).

[26] R. Magnusson, T.K. Taylor, *J. Opt. Soc. Am.* **68**, 809 (1978).

[27] P. Gunter, J.-P. Huignard (Eds.), *Photorefractive Materials and Their Applications I,* Springer-Verlag, Berlin 1988.

[28] M. Klein, *Opt. Lett.* **9**, 350 (1984).

[29] M.S. Petrovic, A. Suchocki, R.C. Powell, G.C. Valley, G. Cantwell, *Phys. Rev. B* **43**, 2228 (1991).

[30] J.I. Pankove, *Optical Processes in Semiconductors,* Prentice-Hall, Englewood Cliffs, N.J. 1971.

[31] R.R. Gerhardts, D. Weiss, K. v. Klitzing, *Phys. Rev. Lett.* **62**, 1173 (1989).

[32] D. Weiss, C. Zhang, R.R. Gerhardts, K. v. Klitzing, *Phys. Rev. B* **39**, 13020 (1989).

[33] P. Vasilopoulos, F.M. Peeters, *Phys. Rev. Lett.* **63**, 2120 (1989).